# Changing climate both increases and decreases European river floods

Günter Blöschl[1†], Julia Hall[†1], Alberto Viglione[1, 12], Rui A. P. Perdigão[1], Juraj Parajka[1], Bruno Merz[2], David Lun[1], Berit Arheimer[3], Giuseppe T. Aronica[4], Ardian Bilibashi[5], Miloň Boháč[6], Ognjen Bonacci[7], Marco Borga[8], Ivan Čanjevac[9], Attilio Castellarin[10], Giovanni B. Chirico[11], Pierluigi Claps[12], Natalia Frolova[13], Daniele Ganora[12], Liudmyla Gorbachova[14], Ali Gül[15], Jamie Hannaford[16], Shaun Harrigan[17], Maria Kireeva[13], Andrea Kiss[1], Thomas R. Kjeldsen[18], Silvia Kohnová[19], Jarkko J. Koskela[20], Ondrej Ledvinka[6], Neil Macdonald[21], Maria Mavrova-Guirguinova[22], Luis Mediero[23], Ralf Merz[24], Peter Molnar[25], Alberto Montanari[9], Conor Murphy[26], Marzena Osuch[27], Valeryia Ovcharuk[28], Ivan Radevski[29], José L. Salinas[1], Eric Sauquet[30], Mojca Šraj[31], Jan Szolgay[18], Elena Volpi[32], Donna Wilson[33], Klodian Zaimi[34], and Nenad Živković[35]

[1]Institute of Hydraulic Engineering and Water Resources Management, Technische Universität Wien, Vienna, Austria
[2]Helmholtz Centre Potsdam, GFZ German Research Centre for Geosciences, Potsdam, Germany
[3]Swedish Meteorological and Hydrological Institute, Norrköping, Sweden
[4]Department of Engineering, University of Messina, Messina, Italy
[5]CSE – Control Systems Engineer, Renewable Energy Systems & Technology, Tirana, Albania
[6]Czech Hydrometeorological Institute, Prague, Czechia
[7]Faculty of Civil Engineering, Architecture and Geodesy, Split University, Split, Croatia
[8]Department of Land, Environment, Agriculture and Forestry, University of Padova, Padua, Italy
[9]University of Zagreb, Faculty of Science, Department of Geography, Zagreb, Croatia
[10]Department of Civil, Chemical, Environmental and Materials Engineering (DICAM), Università di Bologna, Bologna, Italy
[11]Department of Agricultural Sciences, University of Naples Federico II, Naples, Italy
[12]Department of Environment, Land and Infrastructure Engineering (DIATI), Politecnico di Torino, Turin, Italy
[13]Department of Land Hydrology, Lomonosov Moscow State University, Moscow, Russia
[14]Department of Hydrological Research, Ukrainian Hydrometeorological Institute, Kiev, Ukraine
[15]Department of Civil Engineering, Dokuz Eylul University, Izmir, Turkey
[16]Centre for Ecology & Hydrology, Wallingford, Oxfordshire, UK
[17]Forecast Department, European Centre for Medium-Range Weather Forecasts (ECMWF), UK
[18]Department of Architecture and Civil Engineering, University of Bath, Bath, UK
[19]Slovak University of Technology in Bratislava, Faculty of Civil Engineering, Department of Land and Water Resources Management, Bratislava, Slovakia
[20]Finnish Environment Institute, Helsinki, Finland
[21]Department of Geography and Planning & Institute of Risk and Uncertainty, University of Liverpool, Liverpool, UK
[22]University of Architecture, Civil Engineering and Geodesy, Sofia, Bulgaria
[23]Department of Civil Engineering: Hydraulic, Energy and Environment, Universidad Politécnica de Madrid, Madrid, Spain
[24]Department for Catchment Hydrology, Helmholtz Centre for Environmental Research – UFZ, Halle, Germany
[25]Institute of Environmental Engineering, ETH Zurich, Zurich, Switzerland
[26]Irish Climate Analysis and Research Units (ICARUS), Department of Geography, Maynooth University, Ireland
[27]Department of Hydrology and Hydrodynamics, Institute of Geophysics Polish Academy of Sciences, Warsaw, Poland
[28]Hydrometeorological Institute, Odessa State Environmental University, Odessa, Ukraine
[29]Institute of Geography, Faculty of Natural Sciences and Mathematics, Ss. Cyril and Methodius University, Skopje, Republic of Macedonia
[30]Irstea, UR RiverLy, Lyon-Villeurbanne, France
[31]University of Ljubljana, Faculty of Civil and Geodetic Engineering, Ljubljana, Slovenia
[32]Department of Engineering, University Roma Tre, Rome, Italy
[33]Norwegian Water Resources and Energy Directorate, Oslo, Norway
[34]Institute of Geo-Sciences, Energy, Water and Environment (IGEWE), Polytechnic University of Tirana, Tirana, Albania
[35] University of Belgrade, Faculty of Geography, Belgrade, Serbia

* e-mail: bloeschl@hydro.tuwien.ac.at

† These authors contributed equally to this work.

**Abstract**

**Climate change has led to concerns of increasing river floods resulting from the greater water holding capacity of a warmer atmosphere[1]. This concern is reinforced by evidence of increasing economic losses in many parts of the world, including Europe[2]. Any changes in river floods would have lasting implications for designing flood protection measures and flood risk zoning. Existing studies have been unable to identify a consistent continental-scale climatic change signal in flood discharge observations in Europe[3], because of limited spatial coverage and choices in the grouping of hydrometric stations. Here we show that clear regional patterns of both increases and decreases in observed river flood discharges in the last five decades in Europe are evident, which are likely manifestations of a changing climate. Our results suggest that (i) increasing autumn and winter rainfall has led to increasing floods in northwestern Europe, (ii) decreasing precipitation and increasing evaporation have led to decreasing floods in medium and large catchments in southern Europe and (iii) decreasing snowcover and snowmelt as a result of warmer temperatures have led to decreasing floods in eastern Europe. Regional flood discharge trends in Europe range from an increase of +11.4% per decade to a decrease of -23.1%. Notwithstanding the spatial and temporal heterogeneity of the observational record, the flood changes identified here are broadly consistent with climate model projections for the next century[4,5], suggesting that climate-driven changes are already happening, supporting calls for climate change consideration in flood risk management.**

River floods are among the most costly natural hazards. Global annual average losses are estimated at US $104 billion[6], and are expected to increase with economic growth, urbanization and climatic change[2,7]. Physical arguments of increased heavy precipitation resulting from the enhanced water holding capacity in a warmer atmosphere and the occurrence of numerous large floods have exacerbated concerns of increasing flood magnitudes[1]. However, observations of individual extreme events do not necessarily imply that the long-term statistics of flood discharge are also increasing[3].

In Europe, a climatic change signal in flood discharges over the past five decades has been demonstrated in relation to changes in timing of floods within the year[8]. For example, in northeastern Europe, warmer air temperatures have led to earlier spring snowmelt floods. However, changes in flood discharges are still contested, as no coherent large-scale observational evidence has to date been available at the continental scale, due to limited spatial coverage and choices in the grouping of hydrometric stations[3]. A number of studies point towards increases in flood discharges in western Europe in the past five decades. The findings include upward trends in flood discharges in 15% of stations[9], an increase in the occurrence of extreme flood discharges by 44%[10], and significant increases in major-flood occurrence in medium sized catchments[11]. However, these studies are not fully representative as the stations are mainly clustered around western Europe.

Here we analyze the most comprehensive data set of flood observations in Europe[12] to show that a changing climate has increased river flood discharges in some regions of Europe, but decreased floods in others. We base our analysis on river discharge observations from 3738 gauging stations for the period 1960–2010. The catchment areas range between 5 and 100,000 km². For each station, we extracted a series consisting of the highest peak discharge recorded in each calendar year, the annual maximum peak flow. We estimated the trend in each series using the Theil-Sen slope estimator, tested the statistical significance with the Mann-Kendall test, and estimated regional trends by spatial interpolation. We also derived the long-term evolution of floods using a 10-year moving average filter. Finally, we analyzed in a similar fashion the change signal of three plausible drivers of floods: annual maximum 7-day precipitation; highest monthly soil moisture in each year; and spring (January to April) mean air temperature as a proxy for snowmelt and snowfall-to-rain transition. We examined the consistency of changes in drivers with those of floods by comparing the change patterns and by Spearman rank correlation coefficients.

Our data show a clear regional pattern in flood trends across Europe (Fig. 1). Regional trends, relative to the mean flood discharges over 1960-2010, range from an increase of +11.4% to a decrease of -23.1% per decade (Fig. 1). The uncertainties of the regional trends (Extended Data Fig. 2b) are small (typically between 1 and 2% per decade) relative to the spatial signal. Local trends (Extended Data Fig. 2a) at stations range from an increase of +17.8% to a decrease of -28.8% of the long-term station mean per decade. The spatial patterns of trends are grouped into three main regions. In northwestern Europe (Fig. 1, region 1), ~69% of stations show an increasing flood trend (Extended Data Table 2a) with an average local increase of +2.3% per decade. In southern Europe (Fig. 1, region 2), ~74% of stations show a decreasing trend with a regional average trend of -5% per decade. In eastern Europe (Fig. 1, region 3), ~78% of stations show a decreasing flood trend with an average decrease of -6% per decade. In northern Scandinavia and northwestern Russia, trends are less pronounced.

To interpret these changes we focused on seven hotspots of change, where flood trends are particularly clear and flood processes are broadly similar[8] (Extended Data Fig. 2). Because floods result from the interaction between precipitation, soil moisture and snowmelt[13], we analyzed the temporal evolution of these drivers, using air temperature as a surrogate for snowmelt, and compared them to that of floods (Extended Data Fig. 4 a–g). Depending on the region, some of these drivers can be more important than others in explaining flood changes[8].

In the northern UK, floods predominantly result from winter rains associated with high soil moisture[14] (Extended Data Fig. 4a). The increase in flood discharges therefore closely follows increases in winter rainfall and to some degree that of soil moisture (Fig. 2a). This is also shown by statistically significant positive correlations between the temporal variability of flood discharges and these two drivers (Spearman rank correlation coefficient $r$ = 0.70 and 0.36, respectively, Table 1). In western France (Fig. 2b), southern Germany and western Czechia (Fig. 2c), increases in floods are also associated with increases in rainfall, although the correlation with soil moisture is stronger than in the UK, reflecting the important role of soil moisture in flood generation during spring and summer[15] (Extended Data Fig. 4 a-c). In northern Iberia (Fig. 2d), decreasing floods are mainly caused by decreasing winter rainfall, amplified by decreasing soil moisture linked to increasing evapotranspiration[16]. Similarly, in the central Balkans (Fig. 2e), floods have decreased over most of the study period as a result of decreasing precipitation and soil moisture, but the trend appears to have reversed in the 1990s. In southern Finland (Fig. 2f) and western Russia (Fig. 2g), floods usually occur in spring[17], and snowmelt plays an important role. The data show that air temperature has strongly increased (more than 0.5°C per decade) and spring and early summer flood discharges have decreased ($r$ = -0.34 and -0.55, respectively, Table 1), reflecting shallower snow packs, earlier spring thaw (Extended Data Fig. 4f-g), and decreasing snowmelt.

In northwestern Europe (Fig. 1, region 1), increases in extreme precipitation (Fig. 2a-c; Extended Data Fig. 5b) are related to the poleward shift of the subpolar jet and associated storm tracks observed since the 1970s associated with more prevalent positive phases of the North Atlantic Oscillation (NAO) and polar warming[18]. The relationship of NAO variability with polar warming is still debated. Floods in the northern UK hotspot are closely aligned with increasing precipitation resulting in a mean flood discharge trend of +6.6% (Extended Data Table 2c).

In southern Europe (Fig. 1, region 2), the northward shift of the subtropical jet and associated storm tracks[19] as a result of the expansion of the Hadley cell[20] has led to decreasing precipitation, which, together with increasing evapotranspiration[16] related to warmer temperatures, has substantially reduced soil moisture by around 5% per decade (Extended Data Figs. 5b,6b,7b). The combined effect has resulted in decreasing flood discharges in the catchments analyzed here. Small catchments of a few square kilometers are not contained in the data set (the median catchment size of region 2 is about 400 km²), as they are usually not monitored or the flood series are too short for trend analyses. In small catchments, local short-duration convective storms with high intensities are more relevant for flood generation than long-duration synoptic storms, which produce floods in medium and large catchments contained in the data[21]. Local convective storms are expected to increase in a warmer climate[22], which means that floods in small catchments may have actually increased. Additionally, soil compaction, abandoned terraces and land-cover changes may increase flood discharges in small catchments[23]. The difference in catchment size may explain the apparent inconsistency between the occurrence of numerous floods in small catchments in recent years in southern Europe[21]and the decreasing trend in Fig. 1.

In all but southern Europe, increases in extreme precipitation (Fig. 2a–c,f,g; Extended Data Fig. 5b) are related to increased atmospheric blocking associated with decreasing pressure differences between Greenland and the Baltic, which has decreased the speed of zonal (west-east) flow and increased the chance of standing planetary waves[24]. However, it is only in northwestern Europe (Fig. 1, region 1), where the increase in extreme precipitation is reflected in increased flood discharges, as winter storms in that region cause winter floods[8]. Further in the east, snowmelt is more relevant for flood generation.

In eastern Europe, spring air temperature has increased by as much as 1°C per decade (Extended Data Fig. 6b). This has resulted in much less extensive spring snow cover[25], a shift of snowfall to rainfall when air temperatures are around zero, shallower snow packs, earlier snowmelt[8], likely

increased infiltration resulting from shallower freezing depths and therefore smaller floods, even though extreme precipitation in summer has increased[26]. The mean flood trend in the western Russian hotspot is -18.2% (Extended Data Table 2c). Given the colder background temperature (Extended Data Fig. 6a) and larger snowpack in northwestern Russia, the increasing temperatures are not yet changing snowmelt patterns, and hence not decreasing floods (Fig. 1).

While past studies have focused on a few catchments or were clustered around western Europe[9–11,27], this study provides a continental perspective, which allows for an analysis of climate processes that manifest themselves at larger scales. Isolated local or national scale studies, however, are broadly consistent with our findings.

Our results have implications for flood risk management in medium and large sized catchments. The trends shown in Fig. 1 are estimates of changes in the mean annual flood. Since mean annual floods and more extreme floods are usually closely correlated[28], similar trends could also be expected for the 100-year flood, which is often the key design criterion in flood risk management. In northwest Europe (Fig. 1, region 1), flood discharges per unit catchment area (specific flood discharges) are generally high (Fig. 3). For example, on the west coast of the British-Irish Isles and Norway, the specific 100-year flood discharge during the period 1960-2010 was ~0.9 $(m^3/s)/km^2$ (Fig. 3), with floods increasing by ~5% per decade. However, in eastern Europe (Fig 1, region 3), specific flood discharges are rather small (Fig. 3), and are likely to become smaller in a changing climate. For example, in the Baltic countries, southern Poland and the Ukraine, the 100-year flood of ~0.1 $(m^3/s)/km^2$ would decrease to ~0.075 $(m^3/s)/km^2$ if the observed decrease of ~5% per decade persists over the next 50 years. In southern Europe, even if flood discharges decrease in medium and large catchments, discharges are still generally high (Fig. 3), as a result of the proximity to the Mediterranean Sea and associated heavy precipitation events[29]. Floods in small catchments may actually increase as a result of enhanced convective storms[30] and land-use change[23].

Increasing flood discharges imply that, the 100-year flood discharge five decades ago, now has a smaller return period than 100 years, i.e. that discharge is likely to be exceeded on average more often than once in 100 years. In northwestern Europe, what was the 100-year flood discharge in 1960 has now typically become a 50- to 80-year flood discharge (Extended Data Fig. 8), potentially reduction levels of protection offered by existing flood defense structures less safe. In eastern Europe, the 100-year flood discharge has now become a 125- to 250-year flood discharge, which will make structures less economical. While Extended Data Fig. 8, and Fig. 3, do provide a continental overview, they do not replace national-scale and local studies where more detailed information may be available.

It should be noted that the flood trends observed here do not necessarily extrapolate into the future as they may be related to climate variability rather than persistent changes in time[11]. Also, the trends depend on the observation period[3], so may differ if the observation period is extended. However, the regions with a distinct climatic change signal in observed flood discharges identified here are broadly coherent with the projected flood changes in Europe. Most projections for the end of the 21st century suggest increasing floods in (north)western Europe due to increasing precipitation, and decreasing floods in eastern and northern Europe due to increasing temperatures[4,5]. Hence changes in flood discharge magnitudes are already underway, which adds credence to those projections and supports the need to account for climate induced changes in flood risk management.

**References:**

1. IPCC. *Managing the Risks of Extreme Events and Disasters to Advance Climate Change Adaptation. A Special Report of Working Groups I and II of the Intergovernmental Panel on*

*Climate Change*. (Cambridge University Press, Cambridge, UK and New York, NY, USA, 2012).
2. EASAC. European Academies' Science Advisory Council Statement; Extreme weather events in Europe - Preparing for climate change adaptation: an update on EASAC's 2013 study. at <https://easac.eu/publications/details/extreme-weather-events-in-europe/>
3. Hall, J. *et al.* Understanding flood regime changes in Europe: a state of the art assessment. *Hydrol. Earth Syst. Sc.* **18,** 2735–2772 (2014).
4. Kundzewicz, Z. *et al.* Differences in flood hazard projections in Europe-their causes and consequences for decision making. *Hydrol. Sci. J.* **62,** 1–14 (2017).
5. Thober, S. *et al.* Multi-model ensemble projections of European river floods and high flows at 1.5, 2, and 3 degrees global warming. *Environ. Res. Lett.* **13,** 014003 (2018).
6. UNISDR. *Making Development Sustainable: The Future of Disaster Risk Management. Global Assessment Report on Disaster Risk Reduction*. (Geneva, Switzerland: United Nations International Strategy for Disaster Reduction (UNISDR), 2015).
7. Winsemius, H. C. *et al.* Global drivers of future river flood risk. *Nat. Clim. Chang.* **6,** 381–385 (2016).
8. Blöschl, G. *et al.* Changing climate shifts timing of European floods. *Science* **357,** 588–590 (2017).
9. Mangini, W. *et al.* Detection of trends in magnitude and frequency of flood peaks across Europe. *Hydrol. Sci. J.* **63,** 493–512 (2018).
10. Berghuijs, W., Aalbers, E., Larsen, J., Trancoso, R. & Woods, R. Recent changes in extreme floods across multiple continents. *Environ. Res. Lett.* **12,** (2017).
11. Hodgkins, G. A. *et al.* Climate-driven variability in the occurrence of major floods across North America and Europe. *J. Hydrol.* **552,** 704–717 (2017).
12. Hall, J. *et al.* A European Flood Database: facilitating comprehensive flood research beyond administrative boundaries. *Proc. Int. Assoc. Hydrol. Sci.* **370,** 89–95 (2015).
13. Sivapalan, M., Blöschl, G., Merz, R. & Gutknecht, D. Linking flood frequency to long-term water balance: Incorporating effects of seasonality. *Water Resour. Res.* **41,** W06012 (2005).
14. Bayliss, A. C. & Jones, R. C. *Peaks-over-threshold flood database: Summary statistics and seasonality. IH Report No. 121*. (Institute of Hydrology, Wallingford, UK, 1993).
15. Schröter, K., Kunz, M., Elmer, F., Mühr, B. & Merz, B. What made the June 2013 flood in Germany an exceptional event? A hydro-meteorological evaluation. *Hydrol. Earth Syst. Sc.* **19,** 309–327 (2015).
16. Mediero, L., Santillán, D., Garrote, L. & Granados, A. Detection and attribution of trends in magnitude, frequency and timing of floods in Spain. *J. Hydrol.* **517,** 1072–1088 (2014).
17. Hall, J. & Blöschl, G. Spatial patterns and characteristics of flood seasonality in Europe. *Hydrol. Earth Syst. Sc.* **22,** 3883–3901 (2018).
18. IPCC. *2013: Climate Change 2013: The Physical Science Basis. Contribution of Working Group I to the Fifth Assessment Report of the Intergovernmental Panel on Climate Change*. (Cambridge University Press, Cambridge, UK and New York, USA, 2013).
19. Archer, C. L. & Caldeira, K. Historical trends in the jet streams. *Geophys. Res. Lett.* **35,** (2008).
20. Kang, S. M. & Lu, J. Expansion of the Hadley cell under global warming: Winter versus summer. *J. Clim.* **25,** 8387–8393 (2012).
21. Amponsah, W. *et al.* Integrated high-resolution dataset of high-intensity European and Mediterranean flash floods. *Earth Syst. Sci. Data* **10,** 1783–1794 (2018).
22. Ban, N., Schmidli, J. & Schär, C. Heavy precipitation in a changing climate: Does short-term summer precipitation increase faster? *Geophys. Res. Lett.* **42,** 1165–1172 (2015).
23. Rogger, M. *et al.* Land-use change impacts on floods at the catchment scale - Challenges and opportunities for future research. *Water Resour. Res.* **53,** 5209–5219 (2017).
24. Perdigão, R. A. P., Pires, C. A. L. & Hall, J. Synergistic Dynamic Theory of Complex Coevolutionary Systems: Disentangling Nonlinear Spatiotemporal Controls on Precipitation. *arXiv:1611.03403 [math.DS]* (2016).

25. Estilow, T. W., Young, A. H. & Robinson, D. A. A long-term Northern Hemisphere snow cover extent data record for climate studies and monitoring. *Earth Syst. Sci. Data* **7,** 137–142 (2015).
26. Frolova, N. L. *et al.* Hydrological hazards in Russia: origin, classification, changes and risk assessment. *Nat. Hazards* **88,** 103–131 (2017).
27. Mediero, L. *et al.* Identification of coherent flood regions across Europe by using the longest streamflow records. *J. Hydrol.* **528,** 341–360 (2015).
28. Salinas, J. L., Castellarin, A., Kohnova, S. & Kjeldsen, T. Regional parent flood frequency distributions in Europe-Part 2: Climate and scale controls. *Hydrol. Earth Syst. Sc.* **18,** 4391–4401 (2014).
29. Xoplaki, E., Gonzalez-Rouco, J. F., Luterbacher, J. & Wanner, H. Wet season Mediterranean precipitation variability: influence of large-scale dynamics and trends. *Clim. Dynam.* **23,** 63–78 (2004).
30. Brooks, H. E. Severe thunderstorms and climate change. *Atmos. Res.* **123,** 129–138 (2013).

**ACKNOWLEDGEMENTS**

Supported by the ERC Advanced Grant "FloodChange" project (no. 291152), the Horizon 2020 ETN "System Risk" project (no 676027), the DFG "SPATE" project (FOR 2416), the FWF "SPATE" project (I 3174), and a Russian Foundation for Basic Research (RFBR) project (no. 17-05-41030 rgo_a). The data analysis was performed in R using the supporting packages *automap, boot, lattice*, *maptools*, *ncdf4*, *plyr*, *raster, RColorBrewer*, *rgdal* and *rworldmap*. The authors also acknowledge the involvement in the data screening process of C. Álvaro Díaz, I. Borzì, E. Diamantini, K. Jeneiová, M. Kupfersberger, S. Mallucci and S. Persiano during their stays at the Vienna University of Technology. We thank L. Gaál and D. Rosbjerg for contacting Finnish and Danish data holders, respectively; B. Renard (France), W. Rigott (South Tyrol, Italy), G. Lindström (Sweden) and P. Burlando (Switzerland) for assistance in preparing and/or providing data or metadata from their respective regions. We acknowledge all flood data providers listed in Extended Data Table 1.

**Author contributions**

G.B. and J.H. designed the study and wrote the first draft of the paper. G.B. initiated the study. J.H. collated the database with the help of most of the co-authors, and conducted the analyses. A.V. conducted the MCMC analysis. G.B., J.H., A.V., R.P., J.P. and B.M. interpreted the results in the context of underlying geophysical mechanisms. J.P. compiled the catchment boundaries. D.L. contributed to the statistical analysis. M.B., I.Č., A.K., S.K., O.L., M.M.-G., R.M., P.M., I.R., J.L.S., J.S. and N.Ž. interpreted the results in central Europe. G.T.A., A.B., O.B., M.B., A.C., G.B.C., P.C., D.G., A.M., L.M., M.Š., E.V. and K.Z. interpreted the results in southern Europe. B.A., J.J.K. and D.W. interpreted the results in northern Europe. J.H., S.H., T.R.K., N.M., C.M. and E.S. interpreted the results in western Europe. N.F., L.G., A.G., M.K., M.O. and V.O. interpreted the results in eastern Europe. All authors contributed to framing and revising the paper.

**Competing interests** The authors declare no competing interests.

**Correspondence** should be addressed to G.B. (bloeschl@hydro.tuwien.ac.at)

**Table 1 | Spearman's rank correlation coefficient (*r*) between hotspot medians of the annual series of flood discharge and their drivers.** Confidence bounds of *r* are given in Extended Data Table 2b.

| | Northern UK | Western France | Germany Czechia | Northern Iberia | Central Balkans | Southern Finland | Western Russia |
|---|---|---|---|---|---|---|---|
| Precipitation | **0.70 **** | 0.41 * | 0.40 * | **0.54 **** | 0.22 | 0.08 | -0.13 |
| Soil moisture | 0.36 * | **0.57 **** | **0.56 **** | 0.37 * | **0.68 **** | 0.20 | 0.30 |
| Spring temperature | 0.09 † | 0.50 ** † | 0.04 | 0.02 | -0.29 | **-0.34** | **-0.55 **** |

[(**) *p*-value < 0.001, (*) *p*-value < 0.01, † Little snow influence on floods. Bold print indicates largest correlation coefficients in each hotspot.]

**Fig. 1 | Observed regional trends of river flood discharges in Europe (1960–2010).** Blue indicates increasing flood discharges, red decreasing flood discharges (percentage change per decade of the mean annual flood discharge). No. 1–3 indicate regions with distinct drivers: [1] northwestern Europe: increasing rainfall and soil moisture; [2] southern Europe: decreasing rainfall and increasing evaporation; [3] eastern Europe: decreasing and earlier snowmelt. The trends are based on $n = 2370$ hydrometric stations. For uncertainties see Extended Data Fig. 2b.

**Fig. 2 | Long-term temporal evolution of flood discharges and their drivers for seven hotspots in Europe.** (**a**) Northern UK, (**b**) Western France (**c**) Southern Germany and Western Czechia, (**d**) Northern Iberia, (**e**) Central Balkans, (**f**) Southern Finland, (**g**) Western Russia. Observed floods (green), maximum 7-day precipitation (purple), maximum monthly soil moisture (blue), and mean spring air temperature (orange). Solid lines show the median and shaded bands indicate the spatial variability within the hotspots ($25^{th}$ and $75^{th}$ percentile). All data were subjected to a 10-year moving average filter. Vertical axes are indicated in top right corner.

**Fig. 3 | Specific 100-year floods ($(m^3/s)/km^2$) in Europe**, where larger points indicate 90% confidence intervals smaller than 60% of the estimate.

## Methods

### Data sets

The hydrological data used in this study were obtained from a newly created European Flood Database[12], with subsequent updates, containing data from 3738 hydrometric gauging stations from 68 European data sources for the period 1960 to 2010 (Extended Data Table 1). Choice of the study period was guided by a tradeoff between data availability in terms of record length and spatial coverage. The database consists of the highest discharge (daily mean or instantaneous discharge) in each calendar year for each station. For consistency, we chose to analyze the annual maximum flood rather than multiple floods within a year in all stations, as in many areas only annual maxima were available. The stations are located within the domain bounded by 22.25 W – 60.25 E and 34.25 N – 71.25 N (Extended Data Fig. 1), and catchment areas range between 5 and 100,000 km².

The data set was screened for data errors, and catchments that were known, or were identified, to have experienced strong human modifications such as reservoirs that could affect changes in flood

discharges were excluded. The screening involved data pre-selection by co-authors and additional visual examination of the flood records in question, analysis of flood seasonality (jumps in timing and large differences to surrounding stations), and examination of the catchment area in google maps. While local human effects on the floods of individual stations cannot be excluded, the focus of this study was on regionally consistent patterns of change where such effects will not be relevant. In a few catchments, the available flood data had been corrected for the effects of reservoirs to represent near natural flood discharge. In a few cases, local reservoirs may influence the data, but this does not affect the regional pattern. The station density is rather uneven (Extended Data Fig. 1b). In southern Europe it is lower as some stations were removed because of reservoir effects. In Italy, reduced record lengths are related to organizational changes of the hydrographic services[12]. In eastern Europe the density of available stations is generally lower than in other countries and, again, some stations were removed because of reservoir effects.

For estimating the flood discharge trends (Fig. 1 and 2, Extended Data Fig. 2 and 8), only stations that satisfied the following three criteria were considered: at least 40 years of data were available during 1960–2010, the record started in 1968 or earlier, and ended in 2002 or later. In the countries with the highest station densities (Austria, Germany, Switzerland), only stations with at least 49 years of data were included in order to obtain a more even spatial distribution across Europe. In Cyprus, Italy and Turkey, stations with at least 30 years of data were included, and in Spain 40 years of data without restrictions to the start and end of the record. This selection resulted in a set of 2370 stations with a median catchment size of 381 km². Sensitivity analyses indicated that the large-scale spatial pattern of increasing and decreasing flood trends across Europe is not influenced by the choice of record length although the trend of individual stations tends to be sensitive to record length, when increasing the required record length by 5 years, the percentage of significantly positive and negative trends (Extended Data Table 2a) changes only slightly from respectively 11.52% and 16.50% to 11.04% and 16.95%. In this study we evaluated linear trends of the flood discharges. Alternative models of change (e.g. step changes) could also be tested but are beyond the scope of this study.

For each hydrometric gauging station, the contributing catchment boundary was derived from the CCM River and Catchment Database[31]. Daily gridded precipitation sum and mean air temperature data from the E-OBS data set (Version 17.0)[32] for the period 1960–2010 were used. The data consist of interpolated ground-based observations with a spatial resolution of 0.25°. Monthly gridded soil moisture data from the CPC Soil Moisture data set[33] for the period 1960–2010 were analyzed. The data are model-calculated monthly averaged soil moisture water-height equivalents with a spatial resolution of 0.5°.

**Analysis method**

As a first step, we estimated the discharge trend by the Theil-Sen slope estimator[34,35]. The trend estimator $\beta$ is the median slope calculated using the differences of discharge $Q$ over all possible pairs of years ($i$ and $j$, $i < j$) within the time series,

$$\beta = median\left(\frac{Q_j - Q_i}{j - i}\right) \quad (1)$$

where $\beta$ has units of m³/s per year, which was plotted as percentage of the mean flood discharge per decade in Extended Data Fig. 2. The trends were tested for significance by the Mann-Kendall test[36] (Extended Data Table 2a). Some false positives, i.e. detected trends where no trend is present, would be expected because of the large number of stations. The Mann-Kendall test requires the flood discharges to be temporally independent. We therefore tested whether lag 1 autocorrelation exists in the residuals from the trends. 92% of the stations did not exhibit significant lag 1 autocorrelation at the 5% level, suggesting that the Mann-Kendall test is applicable. To identify regional spatial patterns within Europe, $\beta$ was spatially interpolated using the *autoKrige* function

(automatic kriging) of the R *automap* package[37]. The derived trend patterns are plotted in Fig. 1 and in the background of Extended Data Fig. 2a. The uncertainty of the estimated trends at the stations was estimated by bootstrapping[40] and is shown as points in Extended Data Fig. 2b. The uncertainty of the regional trends was estimated as the block kriging standard deviation (kriging error) using the *autoKrige* function and is shown in the background of Extended Data Fig. 2b. The variogram estimated by the function is

$$\gamma(h) = c_0 + c_1\left(1 - \frac{1}{2^{\nu-1}\Gamma(\nu)}\left(\frac{h}{r}\right)^{\nu} K_{\nu}\left(\frac{h}{r}\right)\right) \quad (2)$$

where $h$ is lag, $c_0$= 10.061 (%/decade)², $c_1$= 57.708 (%/decade)², $r$=2394.4 km, $\nu$=0.2 and $K_\nu$ is the modified Bessel function of the second kind. We used block kriging rather than ordinary kriging as we are interested in the uncertainty of the regional estimate rather than that of the local estimate. The uncertainty is evaluated at a 200 x 200 km block size which is the scale at which we suggest Fig. 1 and Extended Data Fig. 2a to be read.

In order to evaluate the robustness of the spatial trend patterns we repeated the interpolation, however, only using stations with significant trends (Extended Data Fig. 3a). The overall pattern is similar to that of the interpolation using all stations (Extended Data Fig. 2a). Additionally, we repeated the interpolation but only using randomly selected stations with distances from each other larger than 50 km to examine the effect of spatial correlations on the trends (Extended Data Fig. 3b). Again, the patterns are similar.

As a second step, we selected rectangular areas or hotspots of change based on similarity of discharge trends and average flood timing as a proxy for flood processes (Extended Data Fig. 2, Extended Data Table 2c). We standardized the flood series of individual stations to zero mean and unit variance to make flood changes within hotspots comparable,

$$Q^0_{i,k} = \frac{Q_{i,k} - \mu_{Q_k}}{\sigma_{Q_k}} \quad (3)$$

where $\mu_{Q_k}$ and $\sigma_{Q_k}$ are the mean and the standard deviation of station $k$, respectively. To compare results between the hotspots we denormalised the flood series of each hotspot $h$ by the mean specific flood discharge $\mu_h$ ((m³/s)/km²) over all years, and the square root $\sigma_h$ of the mean temporal variance,

$$Q^*_{i,k} = \sigma_h Q^0_{i,k} + \mu_h \quad (4)$$

and estimated the long-term evolution in flood discharge with a centered 10-year moving averaging window. We plotted the median of these series within each hotspot (solid lines) and 25th and 75th percentiles of all stations in that hotspot (shaded bands) in Fig. 2. Additionally, the original local flood discharges were tested for significance of a general trend in each hotspot by the Regional Mann-Kendall test[38] (Extended Data Table 2c). Names of hotspots are only indicative and do not correspond to any exactly defined geographic area.

To investigate rain-induced effects on flood changes, we identified for each grid point of the E-OBS dataset the 7-day period with maximum precipitation in each calendar year (with at least 30 years of annual data available). Increases of spring temperatures around or below the freezing point are considered a proxy for snow accumulation, melt and the transition from snowfall to rainfall. To understand the effect of these snowmelt processes on flood discharge, we calculated mean air temperature from January to April. When soil moisture is high, even small rainstorms may produce floods. To understand the effect of high soil moisture on floods, we identified for each grid point of the CPC Soil Moisture dataset the highest monthly soil moisture in each calendar year. We repeated the trend analyses for annual maximum precipitation, spring temperature, and annual maximum monthly soil moisture (Extended Data Fig. 5–7) on a 0.5° grid.

In the hotspot analyses, the time series for these three climate variables were extracted based on their location within the catchment boundaries (or within a buffer distance for small areas), from which Spearman's rank correlation coefficients ($r$) with the spatial medians of the original flood discharge series were calculated (Table 1). Confidence bounds at the 90% confidence level of $r$ were estimated by stochastic block bootstrapping (*boot* package of R, random block size geometrically distributed with mean of 5 years) and are given in Extended Data Table 2b. The long-term evolution of the three climate variables were calculated and plotted in a similar fashion as those of the floods in Fig. 2.

We also analysed changes in the timing of the climate indices and floods as proxies for changing flood processes using previously established methods[8] (Extended Data Fig. 4). The timing is used to interpret the process drivers of flood discharge changes. For Extended Data Fig. 4a, b, d the snow melt index is not shown, as it is of little relevance for flooding[8].

To evaluate the relevance of the observed flood changes for flood management, the 100-year flood ($Q_{100}$) was estimated for each station using a Generalised extreme value (GEV) distribution

$$Q_T = \xi + \frac{\eta}{\kappa} \cdot \left[ 1 - \left( -\ln\left(1 - 1/T\right)\right)^{\kappa} \right] \quad (5)$$

where $Q_T$ is the $T$-year flood discharge. The parameters $\xi$, $\eta$ and κ were estimated from the flood discharge series by Bayesian inference through an MCMC algorithm[39]. Non-informative uniform prior distributions were used for $\xi$ and $\log(\eta)$, while a normal distribution consistent with the geophysical prior[41] were used for κ. 4000 parameter samples were drawn from the posterior distributions from which 4000 100-year floods were calculated for each station by Eq. (5). The median and the relative width of the 90% credible intervals are shown in Fig. 3. For comparability of the 100-year flood in catchments of different sizes, flood discharges per unit catchment area (specific flood discharges; $q_{100}=Q_{100}/A$, where $A$ is catchment area) are shown.

If flood discharges change over time, the return period $T$ may also change, e.g., the 100-year flood may become the 10-year flood if the flood discharges increase. Change in return period was therefore estimated by allowing the parameter $\xi$ in Eq. (5) to change with time $t$ as

$$\xi = a + b \cdot t \quad (6)$$

where the posterior distributions of $a$, $b$, $\eta$ and κ were estimated from the flood discharge series by Bayesian inference through the same MCMC algorithm[39], using non-informative uniform prior distributions for $a$ and $b$. More complex models than (6) were excluded because, for most of the stations, they did not outperform (6) based on the WAIC information criterion[42]. 4000 parameter samples were drawn from the posterior distributions from which 4000 100-year floods in 1960 were calculated for each station by Eqs. (5) and (6) with $t = 1960$. The changed return period in 2010 of these 4000 flood peaks were computed by inverting Eq. (5) and by Eq. (6) with $t = 2010$. Finally, the median of the 4000 return periods was used as the 2010 return period of the 100-year flood discharge in 1960. Those stations where the 5$^{th}$ and the 95$^{th}$ percentiles of the uncertainty distribution agreed in the sign of change, were plotted as large points in Extended Data Fig. 8 while those where this was not the case were plotted as smaller points to indicate the uncertainty involved in the estimation.

To identify large-scale spatial patterns, the logarithms of the 2010 return periods of the 100-year flood discharge in 1960 were spatially interpolated using the *autoKrige* function[37] (Extended Data Fig. 8). For estimating the stationary 100-year specific flood discharge $q_{100}$ (Eq. (5), Fig. 3), less stringent selection criteria (at least 30 years of data) than in all the other analyses were used as it can be estimated more robustly than trends and changes in the return period, which resulted in 3738 stations (Extended Data Fig. 1a).

In this paper we have analyzed flood discharge trends. The flood data set is freely available and can be used for a wide range of analyses.

## References Methods


31. Vogt, J. *et al. A pan-European River and Catchment Database*. *European Commission, Joint Research Centre* (2007).
32. Haylock, M. *et al.* A European daily high-resolution gridded data set of surface temperature and precipitation for 1950-2006. *J. Geophys. Res.* **113,** (2008).
33. Van den Dool, H., Huang, J. & Fan, Y. Performance and analysis of the constructed analogue method applied to US soil moisture over 1981-2001. *J. Geophys. Res.* **108,** (2003).
34. Sen, P. K. Estimates of the Regression Coefficient Based on Kendall's Tau. *J. Am. Stat. Assoc.* **63,** 1379–1389 (1968).
35. Theil, H. A Rank-invariant Method of Linear and Polynomial Regression Analysis, Part 1. *Proc. R. Neth. Acad. Sci.* **53,** 386–392 (1950).
36. Mann, H. B. Nonparametric tests against trend. *Econometrica: Journal of the Econometric Society*, 245-259 (1945).
37. Hiemstra, P. H., Pebesma, E. J., Twenhöfel, C. J. & Heuvelink, G. B. Real-time automatic interpolation of ambient gamma dose rates from the Dutch radioactivity monitoring network. *Comput. Geosci.* **35,** 1711–1721 (2009).
38. Helsel, D. R. & Frans, L. M. Regional Kendall Test for Trend. *Environ. Sci. Technol.* **40,** 4066–4073 (2006).
39. Renard, B., Lang, M. & Bois, P. Statistical analysis of extreme events in a non-stationary context via a Bayesian framework: case study with peak-over-threshold data. *Stoch. Env. Res. Risk A.* **21,** 97–112 (2006).
40. Wilcox, R. A note on the Theil‐Sen regression estimator when the regressor is random and the error term is heteroscedastic. Biometrical Journal: Journal of Mathematical Methods in Biosciences, 40(3), 261-268 (1998).
41. Martins, E. S., & Stedinger, J. R. Generalized maximum-likelihood generalized extreme-value quantile estimators for hydrologic data. Water Resources Research, 36(3), 737-744 . (2000).
42. Watanabe, S. (2010). Asymptotic equivalence of Bayes cross validation and widely applicable information criterion in singular learning theory. Journal of Machine Learning Research, 11, 3571-3594.


## Data Availability

The flood discharge data from the data holders/sources listed in Extended Data Table 1 that were used in this paper can be downloaded from https://github.com/tuwhydro/europe_floods. The precipitation and temperature data from the E-OBS dataset can be downloaded from www.ecad.eu/download/ensembles/ensembles.php. The CPC soil moisture data can be downloaded from www.esrl.noaa.gov/psd.

## Code Availability

The code for the trend and extreme value analyses can be downloaded from https://github.com/tuwhydro/europe_floods.

## Extended Data display items

**Extended Data Figure 1 | Map of European study area.** (**a**) Elevation (m a.s.l.), main rivers and lakes and (**b**) location of the hydrometric stations analyzed. Open and full circles indicate stations with ≥30 years ($n$ = 3738) and ≥ 40 years ($n$ = 2835) of flood discharge data, respectively.

**Extended Data Figure 2 | Observed trends of river flood discharges in Europe (1960–2010).** (**a**) Points show local trends ($n$ = 2370), where larger points indicate statistically significant trends ($\alpha$ = 0.1). Background pattern represents regional trend. Blue indicates increasing flood discharges, red decreasing flood discharges. Rectangles indicate hotspot areas as in Fig. 2, Extended Data Fig. 3 and Extended Data Table 2c. (b) Uncertainties of the trends in terms of standard deviation. Points show local uncertainties. Background pattern represents regional uncertainties at the scale of a block size of 200 x 200 km. Units of both panels are % of mean/decade.

**Extended Data Figure 3 | Flood trends as in Fig. 1 and Extended Data Figure 2, but using fewer stations.** (a) Only stations with significant trends are used (n = 664). (b) Only stations with distances from each other larger than 50 km are used (n = 745).

**Extended Data Figure 4 | Long-term temporal evolution of timing of floods and their drivers for seven hotspots in Europe.** (**a**) Northern UK, (**b**) Western France, (**c**) Southern Germany and Western Czechia, (**d**) Northern Iberia, (**e**) Central Balkans, (**f**) Southern Finland, (**g**) Western Russia. Timing of observed floods (green), 7-day maximum precipitation (purple), snowmelt index (orange), and maximum monthly soil moisture (blue). Lines show median timing and shaded bands indicate variability of timing within the year (±0.5 circular standard deviations). All data were subjected to a circular 10-year moving average filter. Vertical axes show month of the year (June to May).

**Extended Data Figure 5 | 7-day maximum precipitation (1960–2010).** (**a**) Long-term mean (mm/d); (**b**) trends in precipitation (% of mean per decade), where larger points indicate statistically significant trends ($\alpha$ = 0.1); blue indicates increasing precipitation, red decreasing precipitation.

**Extended Data Figure 6 | Spring (January to April) mean air temperatures (1960–2010).** (**a**) Long-term mean (℃); (**b**) trends in temperatures (℃ per decade), where larger points indicate statistically significant trends ($\alpha$ = 0.1); red indicates increasing temperature, blue decreasing temperature.

**Extended Data Figure 7 | Annual maximum monthly soil moisture (1960–2010).** (**a**) long-term mean (mm); (**b**) trends in maximum soil moisture (% of mean per decade), where larger points indicate statistically significant trends ($\alpha$ = 0.1); blue indicates increasing soil moisture, red decreasing soil moisture.

**Extended Data Figure 8 | Estimated return period in 2010 of the discharge that was the 100-year flood in 1960.** Points show local return periods ($n$ = 2370), where larger points indicate agreement of the 5$^{th}$ and the 95$^{th}$ percentiles of the uncertainty distribution in the sign of change. Background pattern represents regional return periods. Blue indicates lower return periods representing increasing flood discharges, red indicates higher return periods representing decreasing flood discharges. This figure provides a continental overview, and does not replace national-scale and local studies where more detailed information may be available.

**Extended Data Table 1 | Data Sources contained in the European Flood Research Database.**

**Extended Data Table 2a | Number of stations with positive and negative flood discharge trends**. Regions according to Fig. 1. [*stations with no trend included]

**Extended Data Table 2b | Estimates and 90% confidence bounds (in brackets) of Spearman's rank correlation coefficient (*r*) between hotspot medians of the annual series of flood discharge and their drivers.** [(**) $p$-value < 0.001, (*) $p$-value < 0.01]

**Extended Data Table 2c | Flood discharge trends for selected hotspots (as % of station mean per decade).** The significance level of the general hotspot trends is given according to the Regional Mann-Kendall test[38] with significance level $\alpha$.

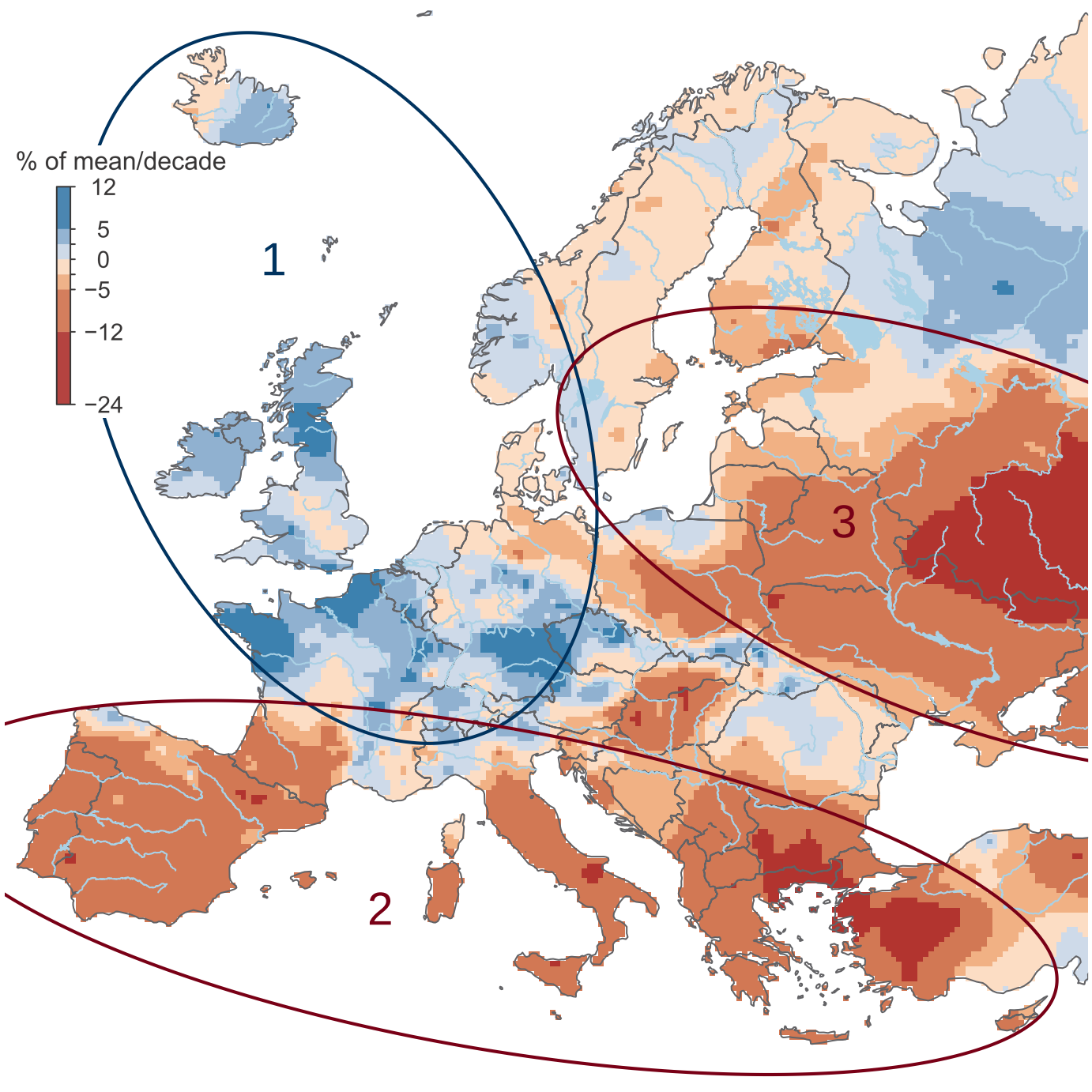
% of mean/decade
12
5
0
−5
−12
−24
1
2
3

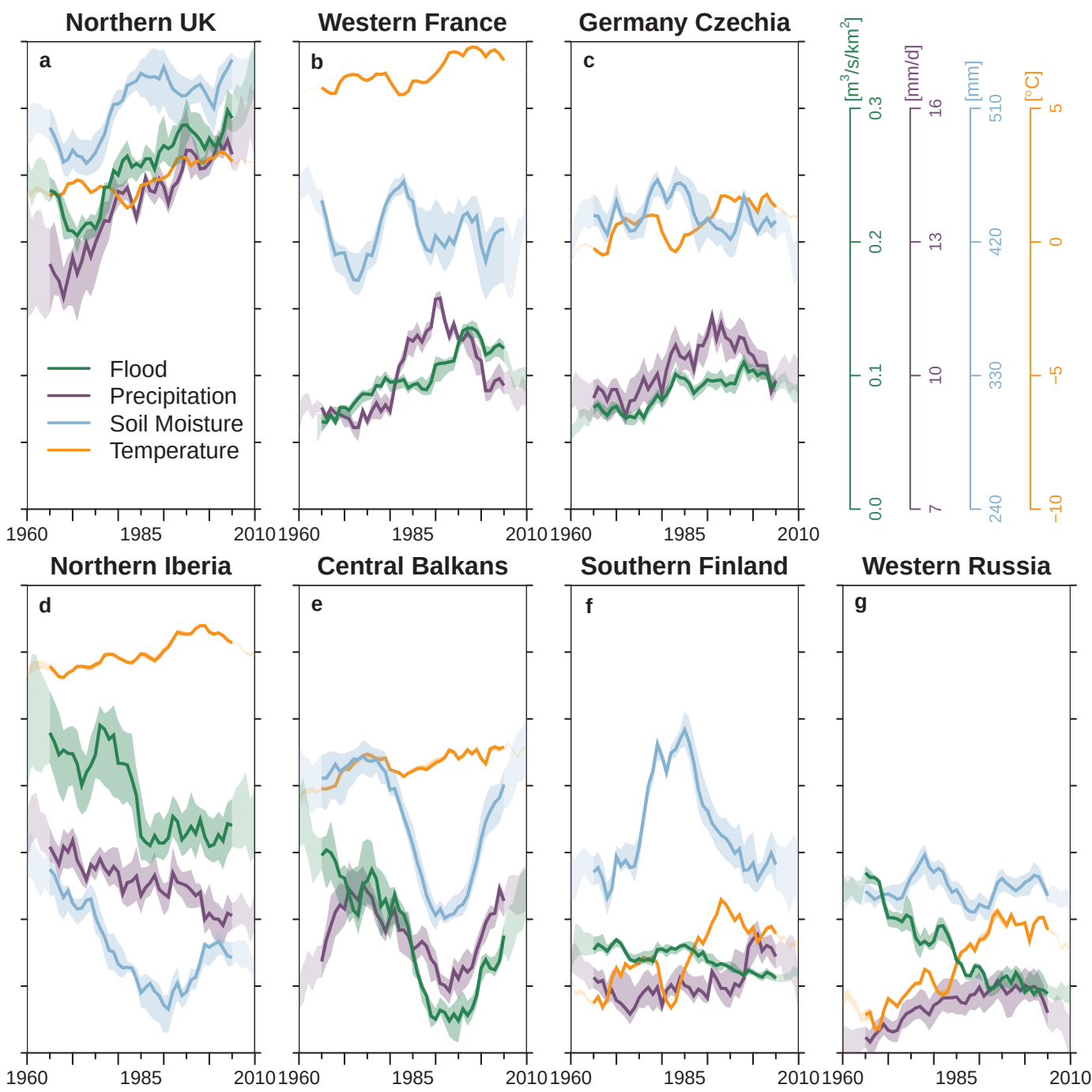
Northern UK
Western France
Germany Czechia
a
b
c
Flood
Precipitation
Soil Moisture
Temperature
[m³/s/km²]
0.0
0.1
0.2
0.3
[mm/d]
7
10
13
16
[mm]
240
330
420
510
[°C]
−10
−5
0
5
1960
1985
2010
Northern Iberia
Central Balkans
Southern Finland
Western Russia
d
e
f
g

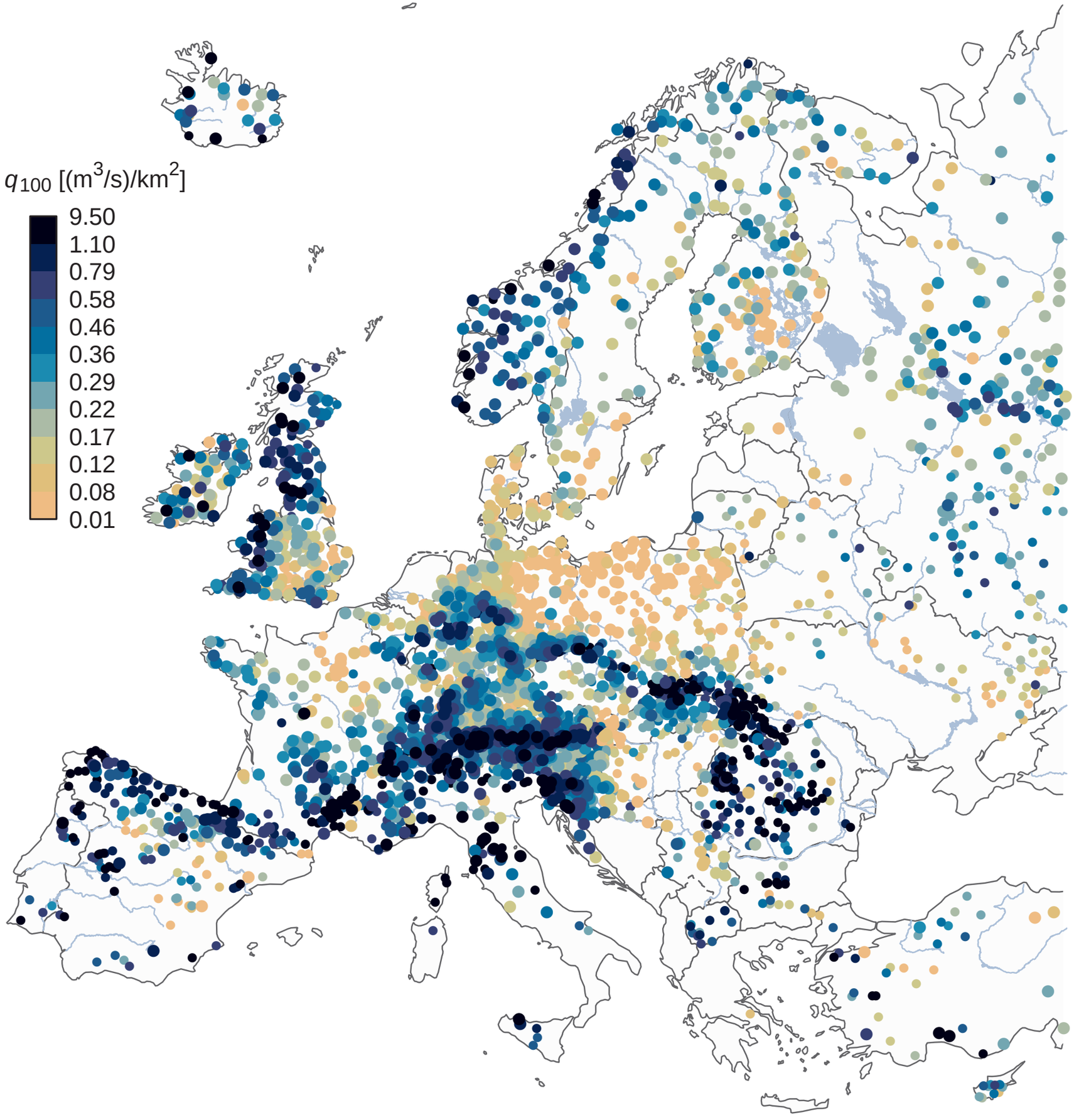
$q_{100}$ [(m$^3$/s)/km$^2$]
9.50
1.10
0.79
0.58
0.46
0.36
0.29
0.22
0.17
0.12
0.08
0.01

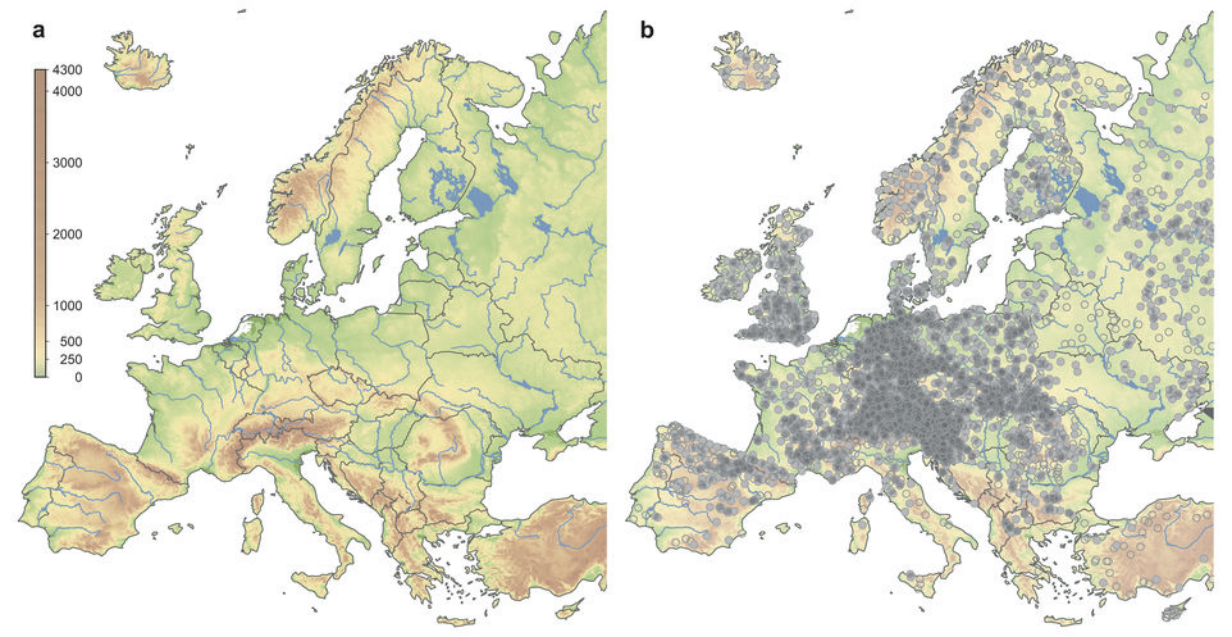
a
4300
4000
3000
2000
1000
500
250
0
b

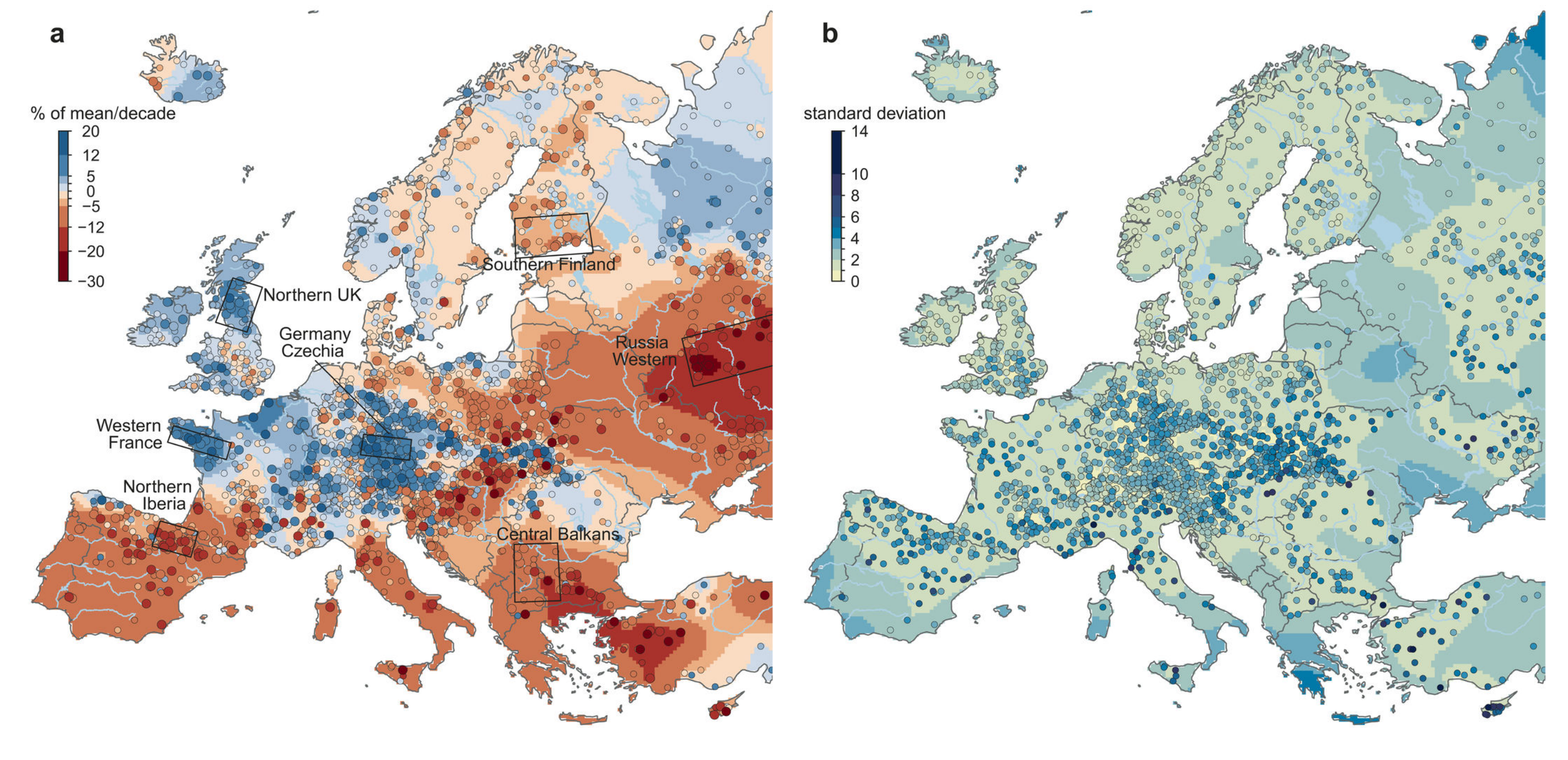
a
% of mean/decade
20
12
5
0
−5
−12
−20
−30
Northern UK
Germany
Czechia
Southern Finland
Russia
Western
Western
France
Northern
Iberia
Central Balkans
b
standard deviation
14
10
8
6
4
2
0

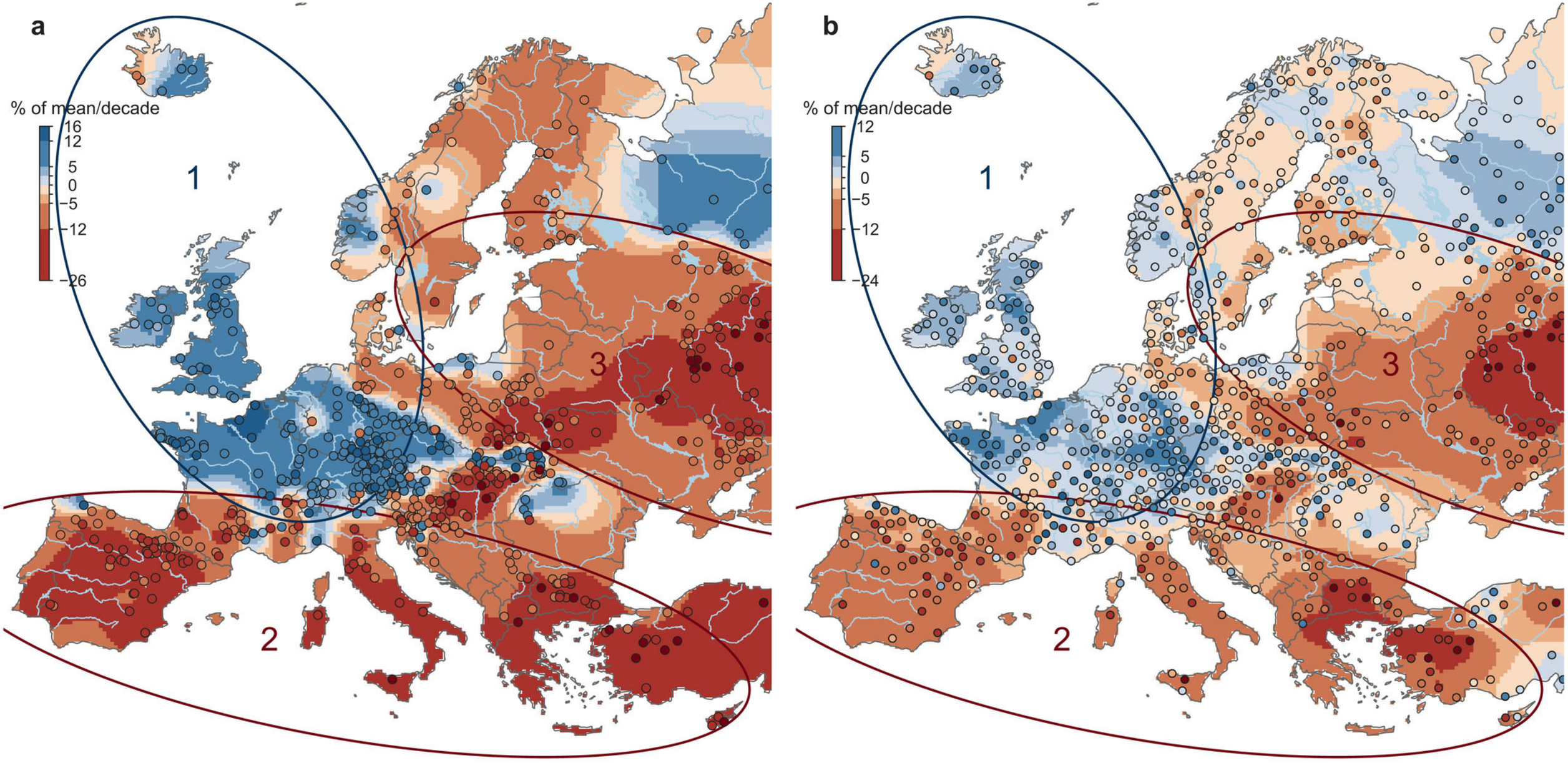
a
% of mean/decade
16
12
5
0
−5
−12
−26
1
2
3
b
% of mean/decade
12
5
0
−5
−12
−24
1
2
3

Northern UK

Western France

Germany Czechia

a

b

c

M A M F J D N O S A J J

1960 1985 2010

Flood

Precipitation

Snow Melt

Soil Moisture

Northern Iberia

Central Balkans

Southern Finland

Western Russia

d

e

f

g

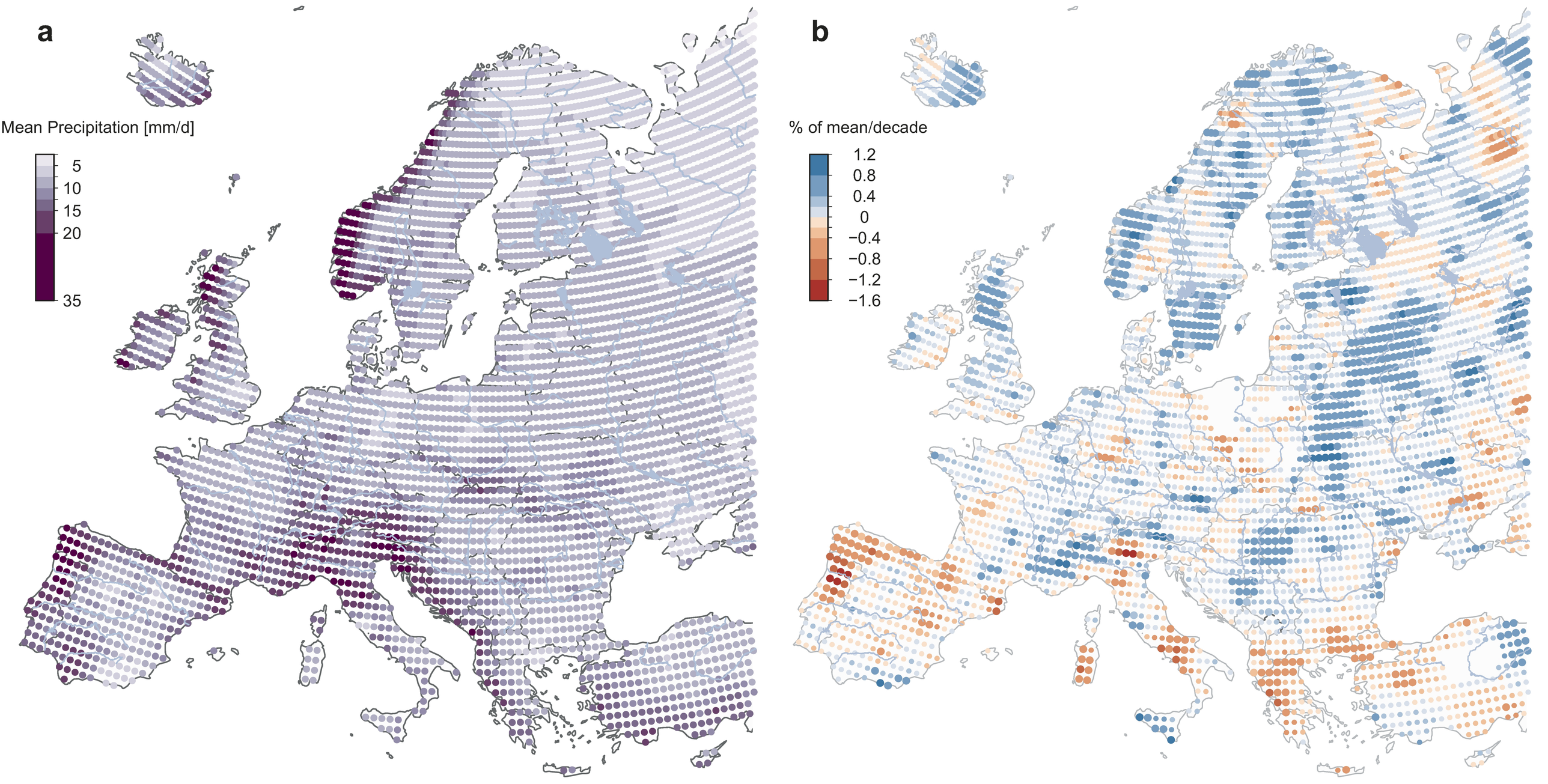
a
Mean Precipitation [mm/d]
5
10
15
20
35
b
% of mean/decade
1.2
0.8
0.4
0
−0.4
−0.8
−1.2
−1.6

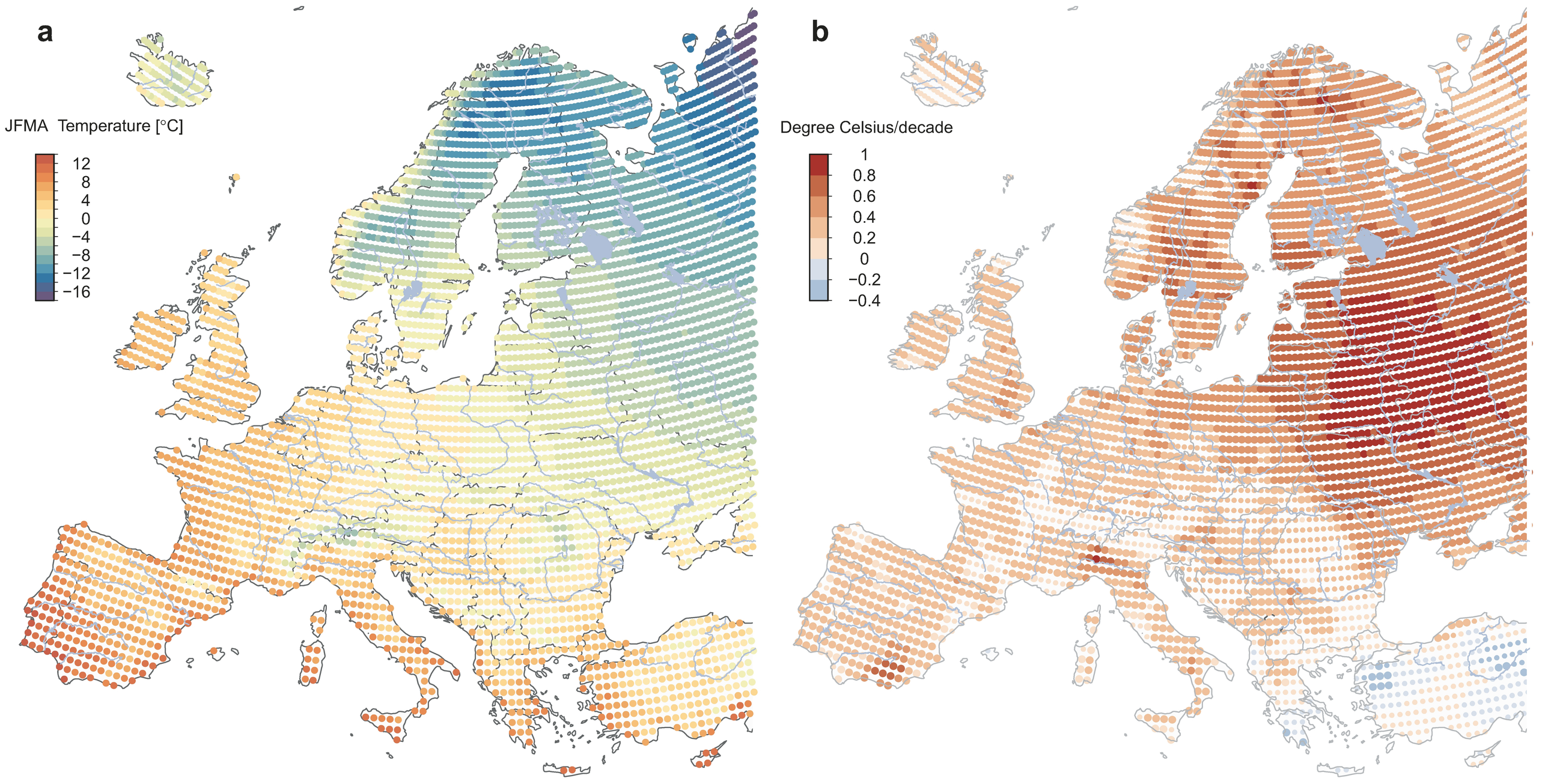
a
JFMA Temperature [°C]
12
8
4
0
−4
−8
−12
−16
b
Degree Celsius/decade
1
0.8
0.6
0.4
0.2
0
−0.2
−0.4

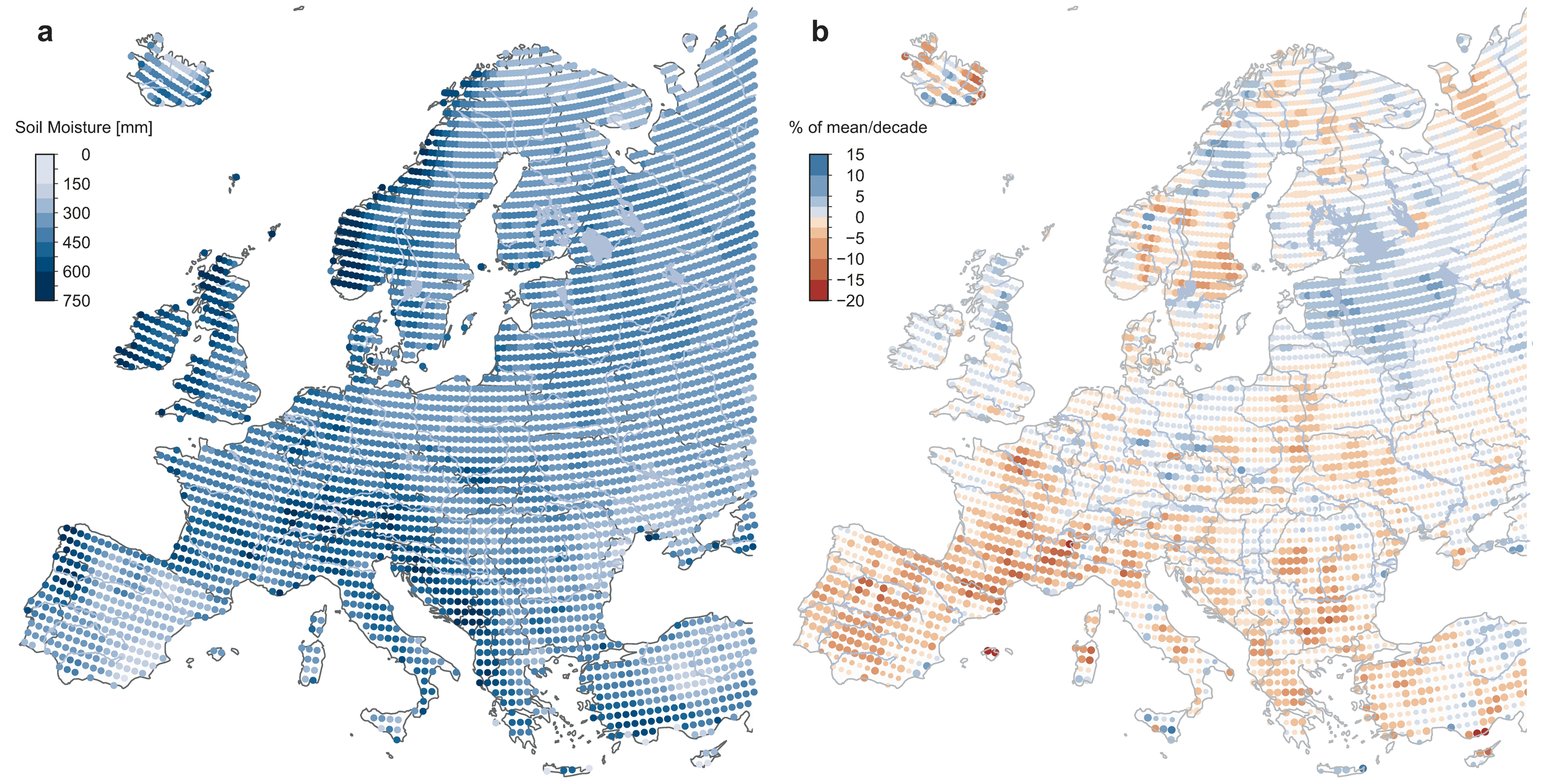
a
Soil Moisture [mm]
0
150
300
450
600
750
b
% of mean/decade
15
10
5
0
−5
−10
−15
−20

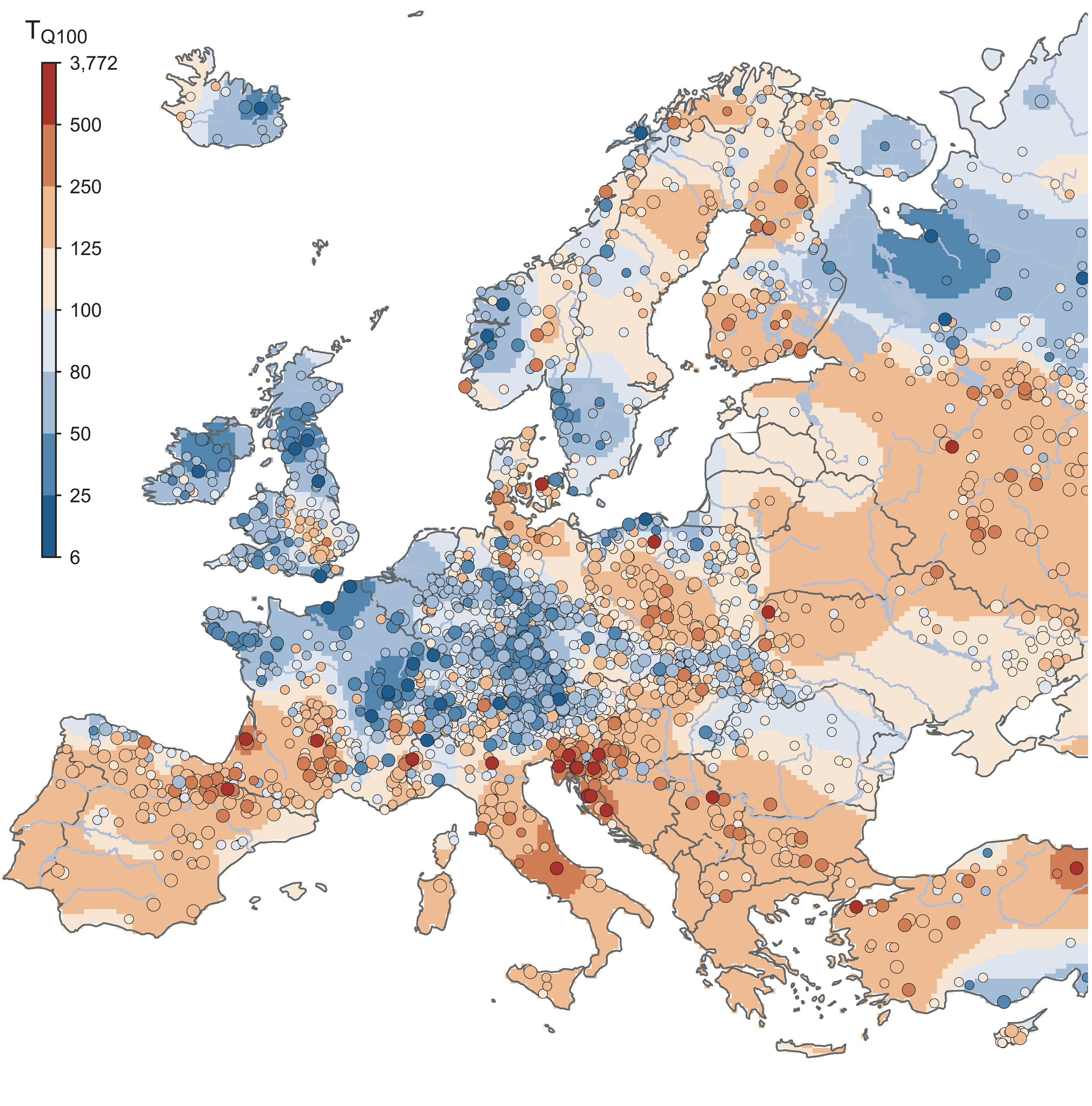
$T_{Q100}$
3,772
500
250
125
100
80
50
25
6

**a)**

| | | Positive Trend | Negative Trend | All |
|---|---|---|---|---|
| **Europe** | **Significant α=0.1** | 273 (11.52%) | 391 (16.50%) | 664 (28.02%) |
| | **Not Significant** | 833 (35.15%) | 837 (35.31%) | 1706 (71.98%)* |
| | **All** | 1106 (46.67%) | 1228 (51.81%) | 2370* |
| **Region 1: North-western Europe** | **Significant α=0.1** | 182 (20.34%) | 27 (3.01%) | 209 (23.35%) |
| | **Not Significant** | 435 (48.60%) | 240 (26.82%) | 686 (76.65%)* |
| | **All** | 617 (68.94%) | 267 (29.83%) | 895* |
| **Region 2: Southern Europe** | **Significant α=0.1** | 13 (2.84%) | 142 (31.00%) | 155 (33.84%) |
| | **Not Significant** | 96 (20.96%) | 169 (42.80%) | 303 (66.16%)* |
| | **All** | 109 (23.80%) | 338 (73.80%) | 458* |
| **Region 3: Eastern Europe** | **Significant α=0.1** | 5 (1.77%) | 115 (40.78%) | 120 (42.55%) |
| | **Not Significant** | 54 (19.15%) | 104 (36.88%) | 162 (57.45%)* |
| | **All** | 59 (20.92%) | 219 (77.66%) | 282* |

**b)**

| | Northern UK | Western France | Germany Czechia | Northern Iberia | Central Balkans | Southern Finland | Western Russia |
|---|---|---|---|---|---|---|---|
| **Precipitation** | **0.70**** (0.57, 0.76) | 0.41* (0.15, 0.64) | 0.40* (0.24, 0.56) | **0.54**** (0.39, 0.68) | 0.22 (-0.11, 0.49) | 0.08 (-0.11, 0.28) | -0.13 (-0.4, 0.18) |
| **Soil Moisture** | 0.36* (-0.01, 0.66) | **0.57**** (0.39, 0.71) | **0.56**** (0.41, 0.68) | 0.37* (0.12, 0.55) | **0.68**** (0.50, 0.76) | 0.20 (0.01, 0.4) | 0.30 (0.07, 0.49) |
| **Spring temperature** | 0.09 (-0.15, 0.25) | 0.5** (0.33, 0.63) | 0.04 (-0.19, 0.23) | 0.02 (-0.23, 0.32) | -0.29 (-0.44, -0.12) | **-0.34** (-0.49, -0.15) | **-0.55**** (-0.7, -0.3) |

**c)**

| Hotspot Name | No. of Stations | Minimum trend | Maximum trend | Mean hotspot trend | Signifi-cance |
|---|---|---|---|---|---|
| **Northern UK** | 15 | 2.9 | 12.5 | 6.6 | α<0.01 |
| **Western France** | 16 | 5.9 | 17.6 | 9.7 | α<0.01 |
| **Germany Czechia** | 47 | 1.6 | 17.8 | 8.0 | α<0.01 |
| **Northern Iberia** | 34 | -18.3 | 3.8 | -8.3 | α<0.01 |
| **Central Balkans** | 15 | -17.6 | -0.1 | -8.4 | α<0.01 |
| **Southern Finland** | 15 | -10.0 | -2.1 | -5.2 | α<0.01 |
| **Western Russia** | 21 | -28.8 | -8.3 | -18.2 | α<0.01 |